View metadata, citation and similar papers at core.ac.uk

brought to you by CORE

provided by White Rose Research Online

This is a repository copy of *A novel method for the analysis of particle coating behaviour via contact spreading in a tumbling drum: Effect of coating liquid viscosity*.

White Rose Research Online URL for this paper:
http://eprints.whiterose.ac.uk/144571/

Version: Accepted Version

Article:
Yusof, N., Green, J., Pitt, K. et al. (5 more authors) (2019) A novel method for the analysis of particle coating behaviour via contact spreading in a tumbling drum: Effect of coating liquid viscosity. Powder Technology. ISSN 0032-5910

https://doi.org/10.1016/j.powtec.2019.03.044

Article available under the terms of the CC-BY-NC-ND licence (https://creativecommons.org/licenses/by-nc-nd/4.0/).

Reuse
This article is distributed under the terms of the Creative Commons Attribution-NonCommercial-NoDerivs (CC BY-NC-ND) licence. This licence only allows you to download this work and share it with others as long as you credit the authors, but you can't change the article in any way or use it commercially. More information and the full terms of the licence here: https://creativecommons.org/licenses/

Takedown
If you consider content in White Rose Research Online to be in breach of UK law, please notify us by emailing eprints@whiterose.ac.uk including the URL of the record and the reason for the withdrawal request.

White Rose university consortium
Universities of Leeds, Sheffield & York

eprints@whiterose.ac.uk
https://eprints.whiterose.ac.uk/

*Corresponding author: Rachel Smith. Email: rachel.smith@sheffield.ac.uk, Tel: +44 (0)114 2228255

A novel method for the analysis of particle coating behaviour via contact spreading in a tumbling drum: Effect of coating liquid viscosity

Norzaida Yusof[1,2], Joshua Green[1], Kate Pitt[1], Omid Arjmandi-Tash[1], Andrew I. Campbell[1], Hossein Ahmadian[3], Hossam Tantawy[3], Rachel Smith[1*]

[1] Department of Chemical and Biological Engineering, University of Sheffield, UK

[2] Faculty of Bioresources and Food Industry, University Sultan Zainal Abidin, Malaysia

[3] Newcastle Innovation Centre, Procter & Gamble, Newcastle, UK

Abstract

Spray coating is a common method of distributing liquids over powders, especially in the pharmaceutical, detergent and food industries. During this process, liquid drops are deposited on the surface of particles. Liquid is then transferred between particles via particle collisions, in a process called liquid contact spreading. This contact spreading process facilitates inter-particle coating, in which wetting, de-wetting, mixing and drying are occurring simultaneously. This work presents the first experimental study of the mechanism of liquid contact spreading. In this work, a novel experimental method has been developed to investigate the mechanism of contact spreading, incorporating a newly developed image analysis technique, based on colourimetric measurements, to quantitatively determine coating behaviour via contact spreading.

Here, experiments designed to isolate the contact spreading coating mechanism were performed in a tumbling drum using a model material system; alumina particles and dyed polyethylene glycol solutions of varying viscosities. The coating uniformity was quantified by the variation in inter-particle coating; the coefficient of variation (CoV). For all systems, the uniformity of the coating increased with time until the CoV decreased to an asymptotic value. The rate of the decrease in the CoV was successfully fitted using an exponential decay function.

The viscosity of the coating solution had a significant effect on the rate of liquid transfer; the lower the viscosity the faster the contact spreading process. This effect is attributed to differences in the formation and stability of liquid bridges between the particles, influencing the extent of liquid transfer. The results also show that in most cases examined here, viscous forces play a main role in the contact

spreading process, and the contribution of capillary forces are minimal. This understanding could assist the design and scale up for the wet coating processes.

Keywords: Contact spreading; Spray coating; Tumbling drum; Coating uniformity; Inter-particle coating; Image analysis

1. Introduction

Spray coating of liquids onto powders and particles is a common process used to develop structured particulate products in numerous industries, including pharmaceuticals, foods, agriculture and detergents. Coatings can be applied to protect particles from incompatible elements, to control the release of active ingredients in core particles, to provide chemical functionality, and to improve appearance, taste and odour, for example. In the coating process, a suspension of atomized droplets is applied to particles agitated in a tumbling drum or fluidised bed; both of which are widely used for coating particles [1]. The aim of this work is to develop an understanding of how liquid viscosity affects the contact spreading of liquids between powders in a tumbling drum, and to show that a specially developed imaging technique is capable of producing reliable and accurate information on the coating variation within a particle batch.

Spray coating of powders may seem a simple process. However, wet coating processes experience complex interactions which involve three state phases; solid, liquid and gas, and cause the design and scale-up of these processes to be based largely on trial and error [2,3]. Spray coating can be conceptually divided into two distinct steps; (i) the initial droplet deposition onto the particle surfaces (Fig. 1a), and (ii) the contact spreading of liquid between particles due to the formation and rupture of liquid bridges (Fig. 1b). Research to date has tended to focus on the droplet deposition mechanism rather than the liquid transfer via contact spreading. However, in tumbling drums, contact spreading is thought to provide a significant contribution [4,5], and understanding this mechanism could assist in design and scale up rules for wet coating processes.

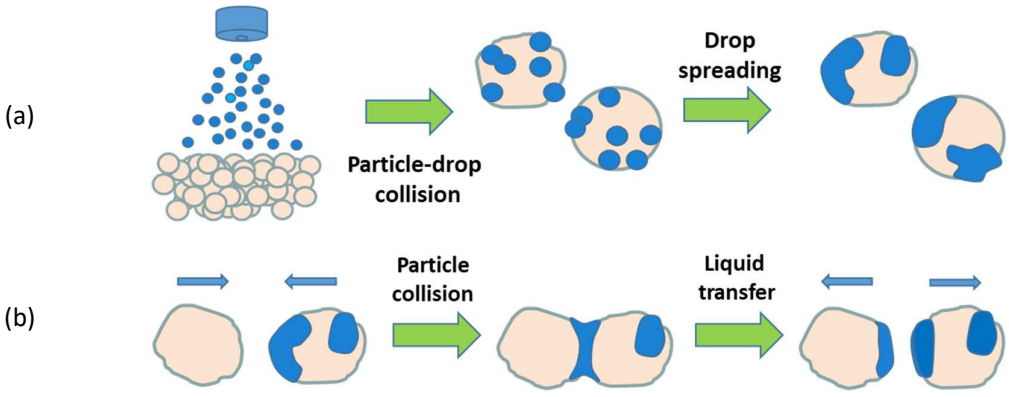

Fig. 1. Spray coating mechanisms: (a) drop deposition (b) contact spreading.

Coating uniformity is one of the most important quality control measures for final products [6-8], which can be described in terms of two coating variations: (i) Intra-particle coating variation, is the coating variation on a single particle; (ii) Inter-particle coating variation, refers to the coating variation between different particles within one batch [9]. Intra-particle coating uniformity is important as the overall performance of a coating may be limited by the thinnest point on the particle. Inter-particle uniformity is important for a homogeneous coating in a batch. Wide variations may have a major impact, particularly for tablets in the pharmaceutical industry. In the case of some tablets in the batch only receiving a small amount of coating, high levels of blood toxicity are possible due to uncontrolled drug release. In contrast, tablets receiving too much coating could cause a delay in drug release.

In order to predict the coating process, it is important to understand the effect of formulation (e.g. particle size [9-11], shape [12], coating solution concentration [13,14]) and operational (e.g. coating time [13-15], spray pattern [13,16], drum velocity [12-14]) variables on coating quality. To quantify the effect of such parameters, analytical techniques are required to investigate the extent of the coating on the particles. Many studies have attempted to characterise the coating layer, using techniques such as batch weight gain [13,17], digital imaging [18,19], X-ray tomography [20,21], confocal laser scanning microscopy [20], laser induced breakdown microscopy [22], atomic force microscopy [23] and scanning electron microscopy [24].

Although the techniques used in the aforementioned studies have proved viable for coating characterisation, many of these studies have mainly focused on intra-particle coating uniformity. They do not adequately characterize the overall coating quality for each batch, i.e. inter-particle coating uniformity, which is a major concern when coating bioactive ingredients. There are, however, other studies which have described methods for quantifying coating variability within a batch of particles

coated in equipment such as tumbling drums and fluidised beds. Many investigations have used simple weight gain [9,10,15,25] or size gain [13,26] of a sample of coated particles taken from a batch in order to determine inter-particle coating variability. For example, Liu and Litster [25] studied the effect of spouted bed process parameters on the mass distribution of seeds coated with fertilizer. Here, a representative sample of 50-100 particles was taken from the final product of each experiment and each particle weighed individually. In a study by Li et al. [10], a combination of weight gain and nuclear magnetic resonance (NMR) was used to determine the coating amount. NMR analyses were performed by measuring a specific component in the coating solution. Image analysis methods have also been used for the characterisation of particle coatings. Kennedy and Niebergall [27] developed a digital imaging system for the assessment of pharmaceutical coatings based on measurement of the optical densities of particles. The standard deviation of the optical density of individual particles was used to evaluate inter-particle coating uniformity. Laser induced breakdown spectroscopy (LIBS) also offers a method of determining inter-particle coating uniformity [8,16,28]. For example, Dubey et al. [28] applied LIBS to study the influence of speed, loading and spray pattern on tablet coating variability in a pan coater and used their results to validate their Discrete Element Method (DEM) simulations. Other spectroscopic methods have also been reported for the determination of inter-particle coating variability [29-32]. Mauer and Leuenberger [32] employed near infrared spectroscopy (NIRS) to determine inter- and intra-tablet variation of samples taken from a pan coater at different time intervals. Romero-Torres et al. [30] investigated the feasibility of using Raman spectroscopy for measurement of tablet-to-tablet coating variability, and concluded it is a simple and robust technique for quantitative characterisation of coating variations. Another method by which to interrogate coating thickness variations is terahertz pulsed imaging (TPI) [32-34]. For example, Lin et al. [34] used this technique to monitor tablet film coating thickness and inter-tablet variability as a function of a variety of process conditions in a pan tablet coater. Microscopy techniques have also been used for the characterisation of coating variation. Andersson et al. [35] used fluorescence microscopy to characterise pharmaceutical pellet thickness and variance between pellets. Confocal laser scanning microscopy (CLSM) has also been employed for determining coating thickness and uniformity [36,37]. For example, Depypere et al. [37] used CLSM to investigate the effect of process settings and coating solution concentration on coating quality of protein coated microparticles in a fluidised bed.

To date there is no single broadly accepted method of characterising inter-particle coating uniformity. While many of these techniques have proven to be capable of characterising inter-particle coating uniformity, most are restricted to the number of particles that can be analysed within a reasonable time frame. Furthermore, many analyses are only suited for characterisation of relatively large-sized

particles and/or high amounts of coating material. Some require time-consuming sample preparation (e.g. fluorescence microscopy) and calibration procedures (e.g. NIRS). Additionally, techniques such as LIBS are destructive, and some microscopy methods require destructive sectioning of the sample particles.

Although extensive research has been conducted into spray coating in drum systems, little research exists which specifically studies the contact spreading mechanism. Indeed, to date studies into contact spreading have been limited to modelling of the process. Shi and McCarthy [4] developed a dynamic liquid transfer model for their DEM studies of heterogeneous particles in a drum spray coating system. Their results showed that the time evolution of coating variability can be fitted with the inverse square root of the time. Mani et al. [38] developed a model based on capillary bridges formed in the pendular regime to study the redistribution of liquid in a sheared unsaturated granular media. They found that the liquid distribution was influenced by the shear rate and the liquid distribution could be inferred indirectly by velocity profiles. Mohan et al. [39] numerically studied the effects of four different liquid transfer models on liquid transfer via inter-particle collisions in sheared particle beds. The study concluded that the fraction of liquid flowing into the bridge was the main contribution to the liquid transfer rate. In 2016, Washino et al [40] proposed a new contact dispersion model for DEM simulations in a spray drum. This differed from the Shi and McCarthy model by taking into account the partial wetting of particles. In the Shi and McCarthy model it was always assumed that particle surfaces were evenly coated with liquid. It was found by Washino et al. that this assumption is only valid for low viscosity coating liquids. However, at higher viscosities, it is necessary to account for partial wetting of the surfaces.

In this paper, we present an experimental study into the contact spreading mechanism. These novel experiments are designed to isolate the rate processes of coating, and allow the investigation of contact spreading in the absence of the spray deposition component. Here, we also use a newly developed qualitative and quantitative image analysis technique, based on colourimetric measurement. This relatively inexpensive method allows the analysis of a relatively large number of particles over a short time period, with minimal sample preparation. Furthermore, it can be used to characterise small quantities of coating material on particles, and has the capability of being employed for a wide range of particle sizes and morphologies. For the first time, we report the use of this experimental technique to investigate the contact spreading process of liquid between particles in a tumbling drum by quantitatively determining coating uniformity as a function of the liquid viscosity. For this study, a model system using alumina beads as the core particles and polyethylene glycols as

the coating solutions is employed to study the effect of coating liquid viscosity on inter-particle coating uniformity.

2. Materials and Methods

2.1. Materials

In this study, alumina beads (Anderman Ceramics Ltd, UK) were used as the model particles (size: d_{10} = 0.88 mm d_{50} = 1.02 mm, d_{90} = 1.18 mm; bulk density = 3.62g/cm^3). Beads were used as supplied, without treatment prior to use. To study the influence of viscosity on contact spreading behaviour, aqueous solutions of polyethylene glycol (PEG) (Sigma-Aldrich, UK) of four different molecular weights (4000, 10000, 20000 and 35000 Da) at the same 50 % wt / wt concentration were used as coating solutions. 1 % wt / wt Acid Red (Sigma-Aldrich, UK) was used to dye the coating solutions to allow for colourimetric characterisation of the coating (see Section 2.3). The physical properties of the solutions are presented in Table 1. The viscosities of the solutions were measured using a rheometer (MCR 502, Anton Paar, Graz, Austria) fitted with a cone and plate (2 ^{o} cone angle, 50 mm diameter), and showed Newtonian behaviour over the applied shear rate (0.1 and 1000 s^{-1}). Surface tension was measured using the Wilhelmy plate technique (KRÜSS tensiometer, GmbH). As expected, the viscosity increases substantially with molecular weight. However, the difference in surface tension between the solutions is minimal.

2.2. Tumbling drum contact spreading experiments

The contact spreading experiments were conducted in a stainless steel tumbling drum, manufactured in-house at The University of Sheffield, with dimensions of 325 mm in length and 210 mm in diameter (Fig. 2), running on a ball mill (Glen Creston, UK). The batch size was 10 % fill level by volume of the drum (2323.7 g). Prior to each run, 10 % of each batch were fully coated with a PEG solution (5 g) of a certain viscosity in a plastic bag outside the drum while the remaining 90 % of uncoated particles were placed in the drum. Subsequently, the fully coated sample was added to the running drum (50 rpm, Froude number = 0.294) using a specifically designed particle delivery device and the timer started. The drum was then stopped after a predetermined time interval and the drum was emptied and the whole batch collected. Runs were then repeated and stopped at increasing time intervals, so as to give a time series of coated batches for the selected coating solution viscosity. Furthermore, for each series, an additional run was performed where the 10 % of the initial coated particles were added into the remainder of the uncoated particles in a static drum without any tumbling and subsequently collected. This experiment quantified any additional liquid transfer from the procedure of emptying the drum and provided an initial start point to the time series. It should be noted that for all batches,

very little of the coating liquid was transferred to the drum surface. Once collected, each of the batches was dried at room temperature (21 °C). This same methodology was used for four different viscosity PEG coating solutions. A minimum of three experiments were performed at each condition to test reproducibility.

It should be noted that coating was completed at durations below 300 s, and the particles for all experiments were still wet at the end of the experiment. While drying will be occurring during the process, the drying in these experiments is unlikely to significantly influence the coating.

Table 1
Properties of the dyed polyethylene glycol (PEG) solutions.

Molecular weight, MW (Da)	Viscosity (mPa.s)	Surface tension (mN/m)
4000	131 ± 30	54.78 ± 0.2
10000	665 ± 90	55.42 ± 0.2
20000	3115 ± 500	55.88 ± 0.2
35000	14903 ± 3000	55.05 ± 0.2

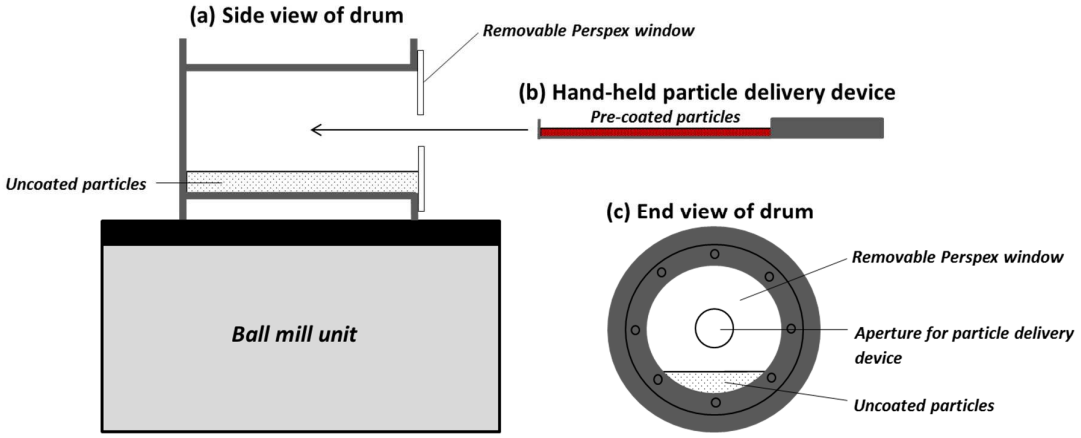

Fig. 2. Tumbling drum experimental set-up.

2.3. Quantitative Image Analysis

After the coating process, a riffled sample of the coated batch was spread on adhesive black vinyl (Anchor Magnets, UK). Subsequently, 24-bit colour images (2752 x 2192 pixels) of the particles were recorded using a Lumenera Infinity 3 Camera (Lumenera Corporation, Canada) fitted with a Navitar 12X zoom lens (Image Optics, UK) and a LGT.19.MF2D LED dome diffuser lamp (Honyu, China). The attached light diffuser incorporates a ring with 120 LEDs which reflect onto a white dome to provide completely shadow free incident illumination, thus reducing reflection on the captured images. A lighting controller was also attached to this light diffuser to provide the correct amount of light required. A typical image featured approximately 150 – 200 beads. Sixteen images were taken for each batch, thereby analysing 2000+ particles per batch. In the case of any overlapping particles, this data was removed from the analysis. To quantify the distribution of the coating on the particles, a set of self-written image analysis LabView algorithms to analyse the colour of the individual particles per batch was used. The 24-bit colour images consist of three 8-bit arrays of pixel values for red, green and blue (RGB) intensities. By identifying the pixels forming the image of an individual particle it is possible to calculate RGB intensity fractions (R + G + B = 1) for each particle and, therefore, how evenly distributed the coating is. For example, where the coating containing the red dye is concentrated on a small number of particles, those particles will have a red intensity fraction greater than 1/3. By determining the relative intensity of the red fraction of the particles, it is possible to quantify changes in the distribution of the coating with processing conditions.

Quantitative analysis of the images began with separating the particles from the image background. After converting the colour image to an 8-bit greyscale image, a boxcar averaging background subtraction algorithm was applied [41]. A fundamental morphological ‘opening’ operation [42] was then employed to ensure the particles are separated from their neighbours in the image. After removing the background and applying LabView’s particle labelling function, an image where the pixels comprising each particle with a unique label was obtained (Fig. 3). The labelled image was then used as a mask to isolate the pixels of each particle in the colour image from which the RGB intensity fractions were calculated. Further details of this process are given in the Appendix.

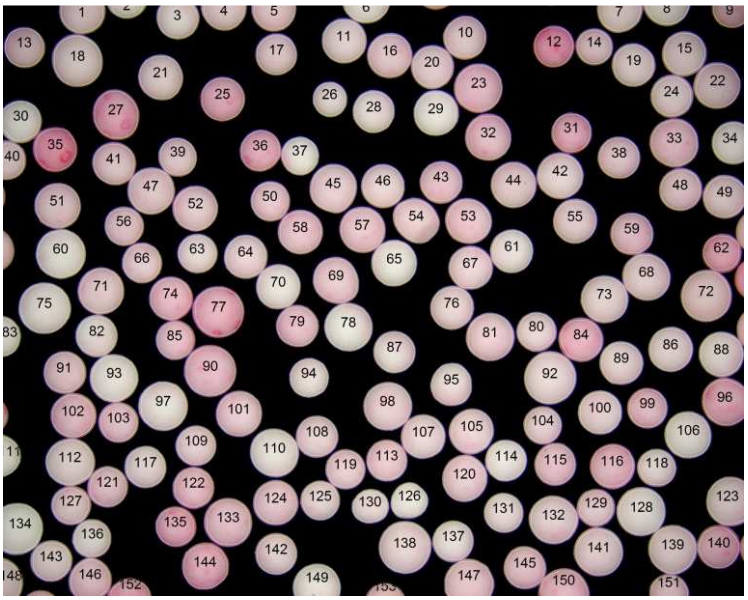

Fig. 3. Labelled image of coated particles.

2.4. Treatment of data

In order to study the effect of coating liquid viscosity on the contact spreading process, an examination of the inter-particle coating variability of each batch series as a function of time was conducted. From the image analysis, values of the mean % red intensity for each particle, and the standard deviation found in this value, were calculated for each data series at every time point. From these values, the coefficient of variation (*CoV*) was calculated as a percentage, as shown in Eq. (1):

$$CoV = \frac{\sigma}{\mu} \times 100 \qquad (1)$$

where μ is the mean % red intensity and σ is the standard deviation of the distribution of % red intensity. The value of the CoV quantifies the coating uniformity within a batch at a certain time point; lower CoV values evidencing a more uniform coating. Values of the CoV were plotted as a function of time for each viscosity series.

3. Results

3.1. Typical data set

In this section, the data analysis procedure is described for a typical coating data set. Here, PEG 10,000 was used as the coating solution (viscosity of 665 mPa.s).

Fig. 4 shows the coating evolution of the alumina particles. Here, a frequency distribution shows the number of particles of differing percentage red values at each time point. The raw particles show a relatively narrow peak at approximately 33.6 % red, indicating that they are virtually white in colour (pure white particles would yield a value of 33.3 %). The pre-coated particles (42.67 % red, σ = 1.83) have a broader distribution of colour. The value of the mean % red is significantly larger than the raw particles enabling us to distinguish between the two. At 0 seconds run time (when the coated particles are added to the drum without any tumbling), there is a shift in the % red to higher values, and a large distribution of red between approximately 33.8 – 43 %. The small peaks at the high % red are attributed to the 10 % initially coated particles. The large, relatively narrow peak at approximately 34.5 % represents the initial 90% uncoated particles. However, there is a shift of the peak of these particles from that of the raw particles to a slightly higher % red, indicating that there is some liquid transfer between particles whilst the drum is being emptied. After 5 seconds, there is a further shift to higher red intensity, with a still relatively large distribution of % red. However, as the time increases, the distributions become narrower indicating less variation in coating with time, i.e. the colour of the batch becoming more uniform due to contact spreading of the coating liquid.

To follow the change in inter-particle coating variability, the CoV value for each time point was determined based on Eq. (1) and plotted as a function of time as shown in Fig. 5. It is observed that the coating variability decreases and the coating becomes more uniform with time, indicating that the process of contact spreading is occurring within the drum. The CoV value for this series appears to reach an asymptotic value of ~1.4 % at approximately 60 seconds. The CoV values were well represented ($R^2 > 0.96$) by the following exponential decay equation, given here as a function of time:

$$CoV(t) = CoV_{\infty} + (CoV_0 - CoV_{\infty})e^{(-\lambda t)} \quad (2)$$

where CoV_{∞} represents the asymptotic variation value in the coating, CoV_0 represents the initial variation at time 0 seconds, λ is the coating rate constant, and t is the tumbling time. The fitted curve can be seen in Fig. 5 for the typical data set.

A regression was performed to fit the data. The fitting constant λ, 0.095 s^{-1} in this case, is a measure of the coating rate. The time for the coating process to reach completion (t_c) is also calculated. As the function is an exponential decay, the time taken to reach complete coating will be infinite. To overcome this, the time for 98 % of the coating to be complete (i.e. $(CoV - CoV_{\infty})/(CoV_0 - CoV_{\infty}) = 0.02$, assuming CoV_0 represents 0 % and CoV_{∞} represents 100 %) is used to determine the characteristic time of coating completion for each of the data sets; given by, $t_c = \ln 0.02/-\lambda$. In the case of this data series, this yields a t_c of 41.17 s.

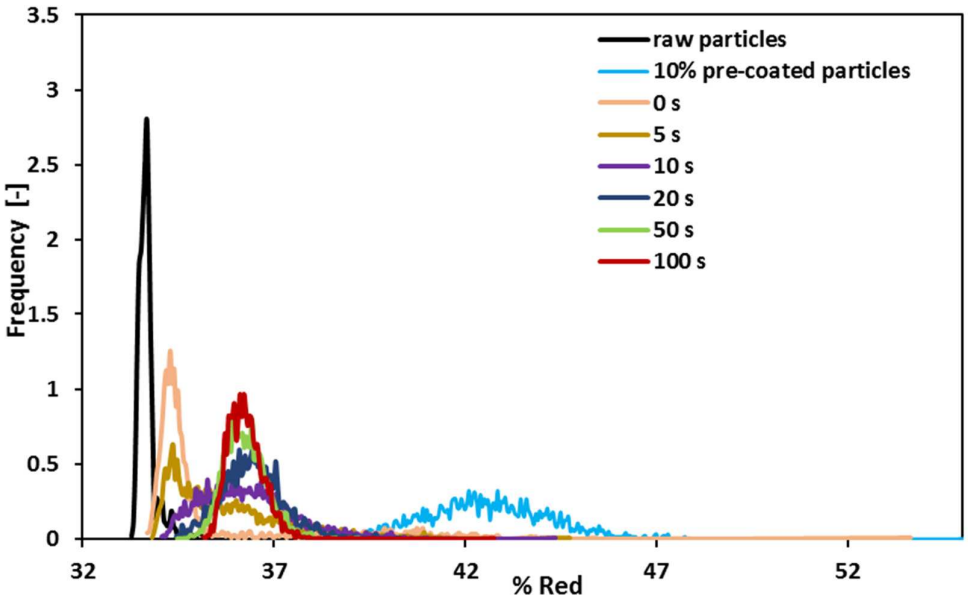

Fig. 4. Coating evolution of alumina particles (note that not all time points for this series are shown for visualisation purposes)

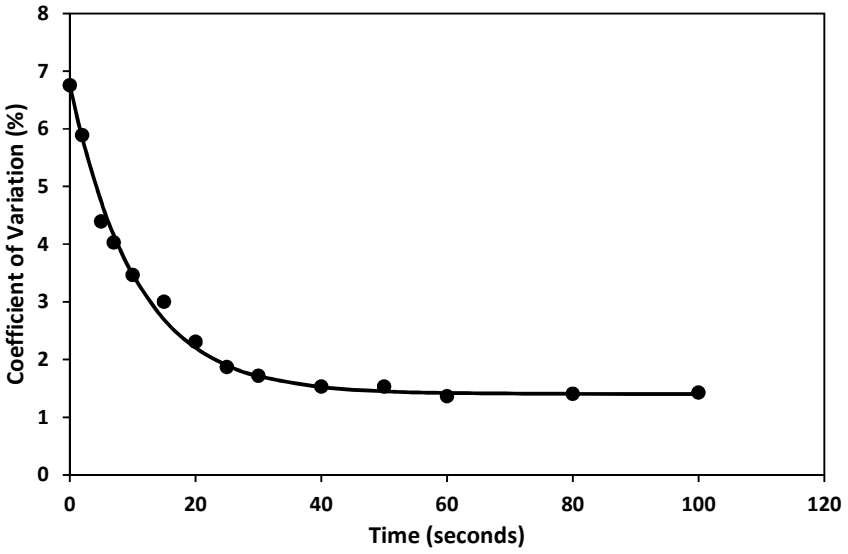

Fig. 5. Raw data represented by circles, and the line is fitted using Eq. (2).

In the following section, this same procedure is used to obtain plots and fitted exponential curves for a series of different coating liquid PEG viscosities, in order to investigate the effect of coating liquid viscosity on the contact spreading process. Coating rate (using the fitted constants, λ) and the time taken for coating completion, t_c, for each series are determined and compared.

3.2. Effect of coating liquid viscosity

Fig. 6 shows all the data sets for the different solution viscosities, fitted with exponential decay curves. The data is normalised according to Eq. (3) for easy comparison of the coating rate for the various solution viscosities.

$$CoV_{Norm} = \frac{CoV(t) - CoV_{\infty}}{CoV_0 - CoV_{\infty}} = e^{(-\lambda t)} \quad (3)$$

From Fig. 6, similar trends were observed for all viscosities, where CoV decreases with time. However, differences in the coating rate constant are exhibited depending on the viscosity of coating solution. The normalised CoV curves are steeper for low viscosity solutions compared to the ones for the higher viscosity coating solutions; this is reflected in their fitting constants (Table 2). Furthermore, the time taken to reach the asymptote, i.e. completion of coating (t_c), is longer for the higher viscosity solutions (Table 2). These differences in coating behaviour when using different coating liquid viscosities could be related to the effect of viscosity on liquid bridge formation, liquid bridge strength, and rupture mechanisms which influence the motion of the particles, as well as the rate of liquid transfer between colliding particles.

The final asymptotic CoV is roughly the same for each of the systems (1.53 ± 0.3), but the rate at which these values are approached varies for each coating solution used. Fig. 7a plots the mean coating rate constants, λ, as a function of coating liquid viscosity. It should be noted that this figure encompasses data from over 100 individual experiments. There is clearly a decrease in the values with increasing viscosity, indicating that contact spreading is a slower process at higher viscosities. Furthermore, the decrease in λ with viscosity appears to be logarithmic; evident by a good fit (R^2 = 0.995) of the fitted logarithmic curve (Fig. 7b). However, a greater number of viscosities would need to be analysed to confirm this relationship. Fig. 8a shows how the time taken for coating completion, t_c, increases as a function of coating liquid viscosity. Fig. 8b shows the log plot of the same data. After being transformed using the earlier developed relationship between λ and t_c ($t_c = \ln(0.02/-\lambda)$, the same equation used to fit Fig. 7 has been used to fit the data in Fig. 8.

Fig. 9 illustrates the images of alumina particles coated with two different viscosities of PEG solution as a function of tumbling time; 131 mPa.s from 10 – 40 seconds (Fig. 9a-c) and 14903 mPa.s from 10 – 140 seconds (Fig. 9d-f). It is visually observed that the variation in coating decreases with time for both viscosities. However, it is clear from the images that the coating process takes longer to yield a uniform coating for the higher viscosity solution; this evidences a slower coating process via contact spreading. These visual studies are in agreement with the quantitative data obtained from the image

analysis. Moreover, for the higher viscosity solution, particularly at low tumbling times, the intra-particle coating variability appears to be higher, compared to the lowest viscosity solution at the same tumbling time. This may be due to the fact that the higher viscosity solutions do not wet as effectively as lower viscosity solutions, or the fact that the liquid bridges are leaving visible localised spots of solution upon rupturing.

Table 2
Extracted fitting parameters and time taken for coating completion for all series of experiments.

Viscosity (mPa.s)	Run	Coating rate constant, λ (s^{-1})	R^2	Time for coating completion, t_c (s)
131	1	0.125	0.988	31.41
	2	0.118	0.979	33.08
	3	0.150	0.987	26.05
	4	0.170	0.998	23.08
	5	0.174	0.988	22.48
	Mean	0.147 ± 0.03	-	27.22 ± 4.0
665	1	0.097	0.983	44.50
	2	0.095	0.994	41.17
	3	0.106	0.984	37.04
	Mean	0.010 ± 0.006	-	40.90 ± 3.0
3115	1	0.081	0.993	48.58
	2	0.077	0.982	50.88
	3	0.072	0.992	54.70
	Mean	0.077 ± 0.005	-	51.39 ± 3.0
14903	1	0.046	0.997	85.46
	2	0.043	0.964	91.16
	3	0.030	0.969	128.68
	4	0.034	0.971	113.99
	5	0.032	0.990	121.28
	Mean	0.037 ± 0.007	-	108.11 ± 19.0

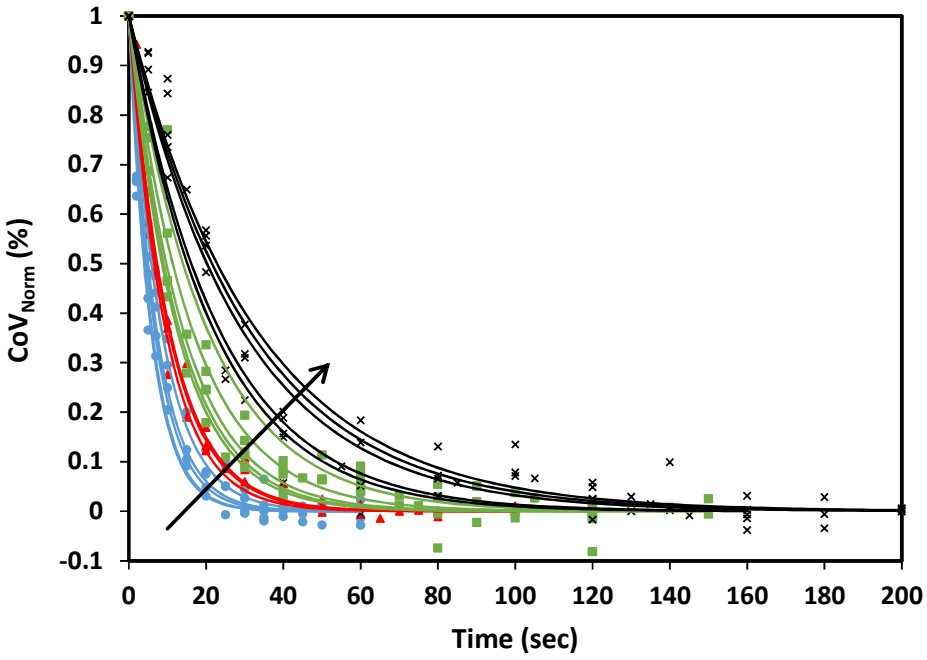

Fig. 6. Normalised CoV and fitted decay curves as a function of mixing time for four different viscosity (μ) PEG solutions (● = 131 mPa.s, ▲= 665 mPa.s, ■ =3115 mPa.s, x = 14903 mPa.s).

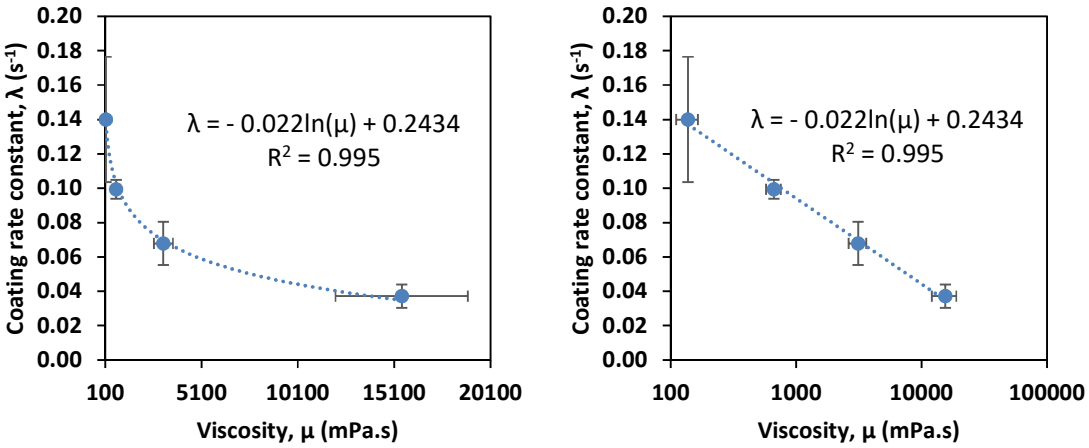

(a) (b)

Fig. 7. Coating rate constants plotted as a function of coating liquid viscosity, a) normal viscosity and b) log viscosity. Error bars represent standard deviation.

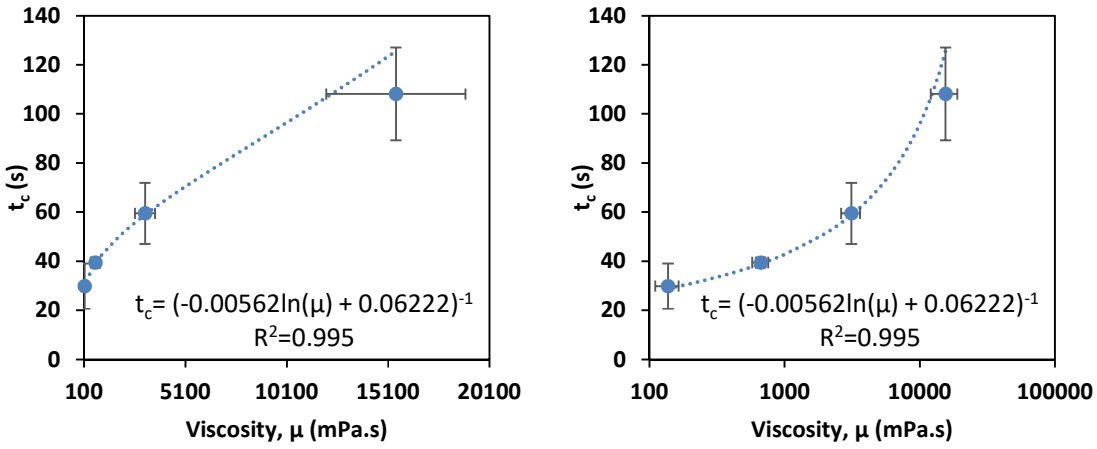

Fig. 8. Time taken for coating completion (t_c) plotted as a function of coating liquid viscosity a) normal viscosity and b) log viscosity. Error bars represent standard deviation.

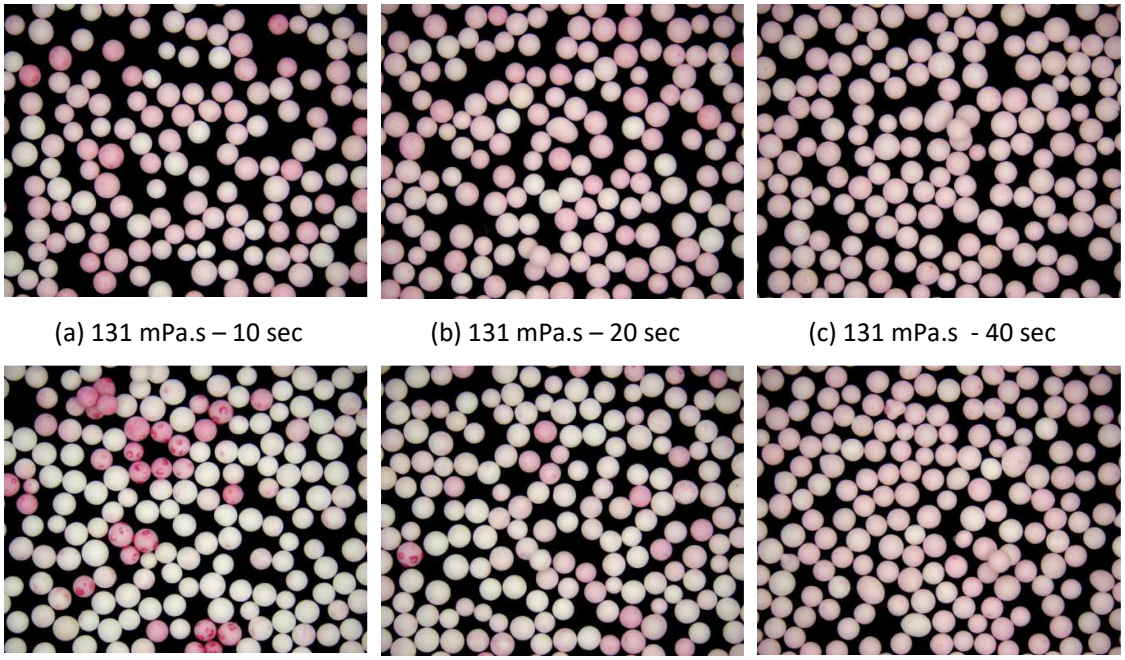

Fig. 9. Images of coated particles as a function of tumbling time at two different PEG viscosities; 131 mPa.s (a) after 10 seconds, (b) after 20 seconds and (c) after 40 seconds; 14903 mPa.s (d) after 10 seconds, (e) after 20 seconds and (f) after 140 seconds.

4. Discussion

In this study, the newly developed technique has been used to quantify the effect of coating liquid viscosity on contact spreading. It is observed that for all viscosities studied, the coating variability decreases and, therefore, by definition, the coating becomes more uniform with time. This is seen from the CoV plots as a function of time (Fig. 6) and also from the colour frequency distributions (Fig. 4), which showed narrower peaks at longer coating times indicating lower colour variability. These results are in agreement with previous experimental [5,13,43] and simulation [26,43] studies for spray coating (including liquid spray), which all reported that the inter-particle coating variability decreases with coating time.

Furthermore, the CoV value appears to reach an asymptotic value. This has been reported by Freireich & Li [44] and Sahni & Chaudhuri [13] in their studies of inter-tablet coating variability. However, it should be noted that these studies involved systems inclusive of liquid spray, so direct comparisons to this present study, where only contact spreading is considered, must be treated with caution. However, in their DEM simulations specific to liquid contact spreading, Shi & McCarthy [4] and Washino et al. [40] reported the attainment of an asymptotic value of coating variability. In our current experimental study, it is expected that the asymptotic CoV value should be the same for each of the systems (allowing for slight variations in liquid colour due to differences in the PEG chain length), and only the rate at which this value is achieved should differ. A zero CoV value represents a perfectly homogenous system; in this study, asymptotic CoV values varied between 1.13 and 1.98, showing minimal but realistic variation from the ideal case. The fact that a zero CoV value is never achieved is probably due to the limitations of mixing in tumbling drums, which have been well-documented (e.g. [5,10,16,26,45]).

To quantify the coating rate, curves were fitted to each data set (CoV as a function of time). As the CoV eventually reached an asymptotic value, exponential decay curves were initially fitted to the data. This fitting method gave excellent fits for all the data sets with an average R^2 value of 0.986 +/- 0.003. Several authors (e.g. [4,43,44]) have fitted their CoV data with a power law function. However, Easo found an exponential relationship using population balance modelling [46]. For this reason, a power law function was also fitted to each of our data sets. Here, the curves could only be fitted from 2 seconds coating time (as the power law function does not hold below 1 second, and 2 seconds was the earliest experimental point considered) and needed an extra fitting parameter. The R^2 values of these fits were then compared with fits using the exponential function, this time adjusted to fit from 2 seconds coating time for direct comparison. An excel solver was used to minimise the sum of the squared difference between the theoretical and actual data points by varying the coating rate

constant, and thereby determine the best fit for each of the functions. The power law also gave good fits to our data sets (R^2 = 0.950 +/- 0.007). However, in all but three cases, the exponential function better fits the decay of the CoV data with time, and the average R^2 value was also slightly higher (0.971 +/- 0.003). Therefore, using the exponential function to fit curves to the data was considered the most appropriate and was employed throughout this work.

From this work, it is clearly evident that coating solution viscosity has a significant effect on the coating rate. This is due to the differing properties of the liquid bridges formed between particles during the process. Many authors have investigated the formation of liquid bridges at the micro-scale, investigating both static and dynamic liquid bridge properties for systems involving two or three particles [47-55]. Liquid viscosity has been shown to have a large impact on the bridge strength, the rupture distance, and the subsequent redistribution of the liquid [56-60]. However, there is currently no research on the effect of liquid viscosity on the coating variation at the process scale, e.g. in a tumbling drum.

Qualitative analysis explains the differences in the CoV values at the early time points. Although the same mass of red dye was added to each solution, the particles seen in Fig. 9 clearly differ in red intensity at the early time points (10 seconds). This effect is amplified at even earlier time points, especially zero seconds, where it is clear that the solutions of increased viscosity have a lower rate of spreading. Fig. 9(d) shows localised spots of intense red colour on individual particles which could be a result of a liquid bridge rupture and slow spreading of the liquid on the particle surfaces. These spots are not visible on images in Fig. 9 (a)(b) or (c), as it presumed that the lower viscosity solutions, even upon bridge rupture, will spread on the solid surface more quickly and not leave localised concentrated spots of solution. The analysis does, however, confirm the trend of increasing coating uniformity with time, and shows the effect that viscosity has on the time scale. This suggests that the current imaging system and software may be an excellent characterization technique for measurement of coating variability.

From images of particles taken during our experiments, partial coverage due to contact spreading is clearly evident at early coating times for both low and high viscosity solutions (Fig. 10). As time progresses, further spreading occurs and the particles become more coated. For PEG with a viscosity of 131 mPa.s, it takes approximately 15 seconds for all the particles to assume complete coverage of PEG and approximately 60 seconds for 14903 mPa.s PEG; although not all particles display the same red intensity and further contact spreading occurs until the asymptote is reached.

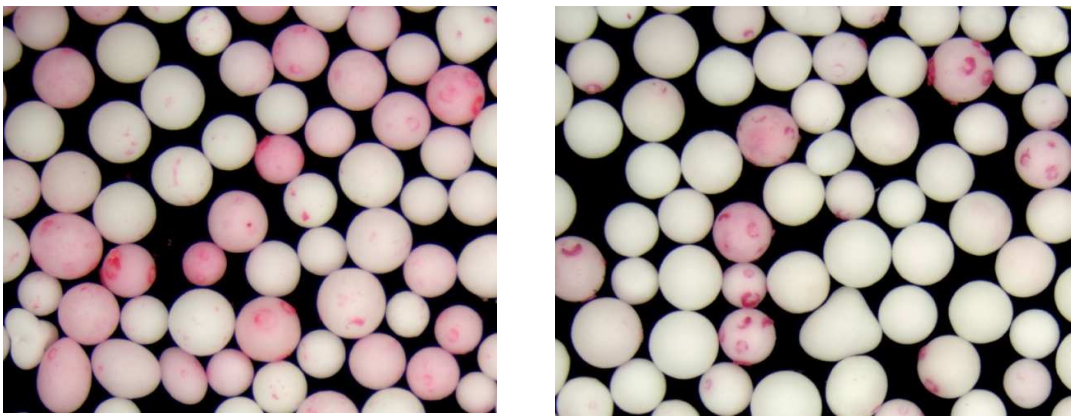

(a) (b)

Fig. 10. Images of particles showing partial coverage (a) 131 mPa.s PEG after 2 seconds (b) 14903 mPa.s PEG after 10 seconds.

As previously mentioned, there have been some modelling studies concerning contact spreading in drum systems. Shi and McCarthy [4] produced a DEM model to incorporate contact liquid spreading, but assumed instantaneous spreading of the liquid over the particle surfaces in the event of a bridge rupture. Washino et al. [40] attempted to improve the model of Shi and McCarthy by segmenting the particle surface, and not assuming instantaneous and full particle liquid coverage. By comparing their results with the Shi and McCarthy model, they found that the assumption of full liquid coverage does not hold for highly viscous fluids. However, their model did not include the ability of the liquid to spread on the particle surface, which in practise would be expected to have a large impact on the liquid redistribution. This is especially true for the systems investigated here, where very slow liquid spreading has been observed, meaning modelling of the system using either of the models described will still under predict the time taken for spreading to occur. Indeed, from the qualitative results of our experiments, seen in Fig. 9 and Fig. 10, this lack of spreading can be seen to particularly influence systems which use high molecular weight PEG solutions. As has been seen, surface tension measurements for each of the four solutions are extremely close in value, indicating any changes in the coating process are due to differences in the liquid viscosity and/ or the surface spreading of the liquids which may depend on the molecular weight of the PEG used.

The difference in coating rate when using different coating liquid viscosities could be related to the different particle dynamics and mixing patterns due to different liquid bridge strength. Wet particles encounter capillary and viscous forces resisting motion. A capillary number, representing the ratio of viscous to capillary forces, was calculated for each of the solutions:

$$Ca = \frac{U\mu_L}{\gamma_L} \tag{4}$$

where U is the characteristic velocity (here, the linear velocity at the periphery of the drum), μ_L is the liquid viscosity, and γ_L is the liquid surface tension. The capillary number is used here to determine the dominant force (capillary or viscous force) on the strength of a dynamic pendular liquid bridge between the particles [61]. A capillary number of 1 indicates the capillary and viscous forces are equally important, whereas a capillary number significantly greater than 1, seen for the majority of the solutions used (Table 3), indicates that viscous forces dominate as a result of either high liquid viscosity or large relative velocity between the particles [62]. These forces can be several orders of magnitude greater than the capillary force [40,56,59]. For the three highest viscosity solutions used here, the capillary force can, therefore, be neglected, and the liquid bridge strength can be approximated by its viscous component, given by Eq. (5) (normal direction) and Eq. (6) (tangential direction) [62]. Although the 131 mPa.s solution has a Ca number of only slightly above 1, for simplicity, and due to the small liquid bridge force relative to the other systems in this work, the capillary contribution was not included in the bridge force calculation.

$$F_{v_n} = 6\pi\mu R^* v_n \frac{R^*}{S} \tag{5}$$

$$F_{v_t} = \left(\frac{8}{15}\ln\frac{R^*}{S} + 0.9588\right) 6\pi\mu R^* v_t \tag{6}$$

In Eq. (5) and Eq. (6), $1/R^* = 1/R_1 + 1/R_2$ where R_1 and R_2 are the radii of the two particles. μ is the fluid viscosity, v is the relative velocity of the spheres (normal and tangential), and S is the separation distance between particles. This first order dependence shows that liquid viscosity can have a large impact on the liquid bridge strength, particle dynamics, and therefore, the rate of contact spreading. A higher viscosity liquid provides more resistance to particle motion and consequently it decreases the frequencies of particle collisions, liquid bridge formations and subsequent ruptures and, thus, the rate of contact spreading. The effect of varying surface tension was not investigated in the current work, and it can be seen in Table 1 that the surface tension for all the liquids used are very similar, with no significant difference between them.

Table 3
Capillary number calculated for each solution.

Viscosity (mPa.s)	Capillary number
131	1.31
665	6.59
3115	30.6
14903	149

The resistance to particle motion, a phenomenon caused by the liquid viscosity, and the kinetic energy of the particles in collisions, are in direct competition. The viscous Stokes number represents the ratio between these two forces and along with a critical Stokes value, determines the likelihood of agglomeration and coating in liquid-powder processing operations [63]. The critical Stokes value is difficult to calculate, as it is a function of the liquid height on the particle, surface asperity height, and the particle coefficient of restitution. The Stokes number can be accurately calculated in cases where the particles' collisional velocities are known. Measuring particle velocities in these systems is a huge challenge, however the linear velocity at the periphery of the drum can be used here as a rough approximation [61,64]. On an individual collision basis, increasing solution viscosity results in a smaller Stokes number. When the value of the Stokes number is below the critical value, the particle collision no longer possesses the energy required to overcome the viscous resistance. It is important to note that within the drum, there are many collisions, and each collision will have a different value of Stokes number, resulting in a distribution of Stokes numbers over the course of a coating process. Therefore, decreasing the viscosity results in a greater proportion of the particle collisions with Stokes numbers above the critical Stokes value, and hence separating upon collision, redistributing the liquid around the bed via contact spreading.

Furthermore, the viscosity of coating liquid directly affects the liquid transfer rate during liquid bridge formation and the rupture process. For a low viscosity liquid, the bridges may achieve equilibrium profiles at all times, which are governed by the contact angle and wettability of two particles in contact [4]. However, in the case of high liquid viscosity, the bridges may not have enough time to achieve an equilibrium profile before rupturing due to a low liquid spreading rate. This, in turn, decreases the amount of liquid distributed between the particles and the rate of contact spreading. Accordingly, it increases the time at which the asymptotic CoV of the system is approached.

5. Conclusion

For the first time, an experimental method to quantify liquid contact spreading in a tumbling drum has been developed. The imaging technique, based on colourimetric analysis, has been used to quantitatively describe the effect of coating liquid viscosity on the contact spreading mechanism in a model liquid-powder system. This newly developed imaging system is capable of handling a significant number of particles, and measurements and analysis can take place in a short period of time. The novel contact spreading isolating experimental technique developed in this study allows several important parameters to be ascertained; the asymptotic CoV value, the time taken to reach this value, and the rate of coating.

This technique has proved successful in mapping the contribution of contact liquid spreading to coating kinetics for a variety of solution viscosities. The lower the viscosity, the faster the contact spreading process, with a shorter time required to reach an asymptotic value of the coefficient of variation. This is attributed to differences in the viscous component of the liquid bridge strength between particles, which influences the mechanism of liquid transfer via contact spreading.

The same methodology has the potential to be applied to investigate other material properties and operational parameters. Industries often resort to iterative, trial and error methods to design their spray coating process. Design and scale up of equipment is a time consuming and difficult process, resulting in large costs. This technique provides insight into the source and timescales for coating uniformity, with applicability to many equipment geometries across industries such as pharmaceuticals, detergents, agrochemical and food. This work is the first experimental step towards a mechanistic understanding of contact spreading, which will ultimately aid the design and scale up of coating processes.

Acknowledgements

This work was supported by the Engineering and Physical Sciences Research Council (EPSRC) IIKE Award, The Royal Society Industry Fellowship (Grant number: IF140095), METRC (Grant number: M1319), Procter & Gamble, the Ministry of Higher Education Malaysia and the University of Sultan Zainal Abidin. The authors would also like to thank Andy Patrick, David Palmer and Sam Cripps (Engineering Workshop, Department of Chemical and Biological Engineering, University of Sheffield) for the manufacture of the tumbling drum, and Dr Oleksandr Mykhaylyk and Dr Matthew Derry (Department of Chemistry, University of Sheffield) for use of the rheometer.

References

[1] K. Saleh, P. Guignon, Coating and encapsulation processes in powder technology, in: A. Salman, M. Hounslow, J.P.K. Seville (EDs.), Granulation, Elsevier Science, 2006, pp.323-375.

[2] R. Turton, X.X. Cheng, The scale-up of spray coating processes for granular solids and tablets, Powder Technol. 150 (2005) 78–85.

[3] L. Suhrenbrock, G. Radtke, K. Knop, P. Kleinebudde, Pellet layering: scale-up considerations using different kinds of processing equipment, Drug Dev. Ind. Pharm. 38(12) (2012) 1494-1503.

[4] D. Shi, J.J. McCarthy, Numerical simulation of liquid transfer between particles, Powder Technol. 184 (2008) 64-75.

[5] G. Toschoff, J. Khinast, Mathematical modelling of the coating process, Int. J. Pharm. 457 (2013) 407-422.

[6] E. Sahni, B. Chaudhuri, Experimental and modeling approaches in characterizing coating uniformity in a pan coater: A literature review, Pharm. Dev. Technol. 17(2) (2012) 134–147.

[7] R. Turton, Challenges in the modeling and prediction of coating of pharmaceutical dosage forms, Powder Technol. 181(2) (2008) 186–194.

[8] M.D. Mowery, R. Sing, J. Kirsch, A. Razaghi, S. Bechard, R.A. Reed, Rapid at-line analysis of coating thickness and uniformity on tablets using induced breakdown spectroscopy, J. Pharm. Biomed. Anal. 28 (2002) 935-943.

[9] S. Tobiska, P. Kleinebudde, Coating uniformity and coating efficiency in a Bohle Lab-Coater using oval tablets, Eur. J. Pharm. Biopharm. 56(1) (2003) 3–9.

[10] J. Li, C. Wassgren, J.D. Litster, Multi-scale modeling of a spray coating process in a paddle mixer/coater: the effect of particle size distribution on particle segregation and coating uniformity, Chem. Eng. Sci. 95 (2013) 203–210.

[11] J. Li, B.J. Freireich, C.R. Wassgren, J.D. Litster, Experimental validation of a 2-D population balance model for spray coating processes, Chem. Eng. Sci. 95 (2013) 360-365.

[12] W.E. Wilson, E. Crossman, The influence of tablet shape and pan speed on intra-tablet film coating uniformity, Drug Dev. Ind. Pharm. 23(12) (1997) 1239-1243.

[13] E. Sahni, B. Chaudhuri, Experiments and numerical modeling to estimate the coating variability in a pan coater, Int. J. Pharm. 418 (2) (2011) 286-296.

[14] J. Wang, J. Hemenway, W. Chen, D. Desai, W. Early, S. Paruchuri, S-Y Chang, H. Stamato, S. Varia, An evaluation of process parameters to improve coating efficiency of an active tablet film-coating process, Int. J. Pharm. 427(2) (2012) 163–169.

[15] R.K. Chang, M. Leonzio, The effect of run time on the inter-unit uniformity of aqueous film coating applied to glass beads in a hi-coater, Drug Dev. Ind. Pharm. 21(16) (1995) 1895-1899.

[16] A. Dubey, R. Hsia, K. Saranteas, D. Brone, T. Misar, F. Muzzio, Effect of speed, loading and spray pattern on coating variability in a pan coater, Chem. Eng. Sci. 66(21) (2011) 5107–5115.

[17] E. Abe, N. Yamada, H. Hirosue, H. Nakamura, Coating mass distributions of seed particles in a tumbling fluidized bed coater, Powder Technol. 97 (1998) 85-90.

[18] M. Mozina, D. Tomazevic, S. Leben, F. Pernus, B. Likar, Digital imaging as a process analytical technology tool for fluid bed pellet coating process, Eur. J. Pharm. Sci. 41(1) 2010 pp.156-162

[19] C.C. Larsen, J.M. Sonnergaard, P. Bertelsen, P. Holm, Validation of an image analysis method for estimating coating thickness on pellets, Eur. J. Pharm. Sci. 18 (2003) 191-196.

[20] F. Sondej, A. Bück, E. Tsotsas, Comparative analysis of the coating thickness on single particles using X-ray micro-computed tomography and confocal laser-scanning microscopy, Powder Technol. 287 (2016) 330–340.

[21] G. Perfetti, E. Van de Casteele, B. Rieger, W.J. Wildeboer, G.M.H. Meesters, X-ray micro tomography and image analysis as complementary methods for morphological characterization and coating thickness measurement of coated particles, Adv. Powder Technol. 21(6) (2010) 663–675.

[22] Y. Mouget, P. Gosselin, M. Tourigny, S. Bechard, Three-dimensional analyses of tablet content and film coating uniformity by laser-induced breakdown spectroscopy (LIBS), Am. Lab. 35(4) (2003) 20.

[23] M. Kalab, P. Allan-Wojtas, S.S. Miller, Microscopy and other imaging techniques in food structure analysis, Trends Food Sci. Technol. 6(6) (1995) 177-186.

[24] J. Heinamaki, M. Rutsalainen, V.M. Lehtola, O. Antikainen, J. Yliruusi, Optimization of aqueous-based film coating of tablets performed by a side-vented pan coating system, Pharm. Dev. Technol. 2 (1997) 357-364.

[25] L.X. Liu, J.D. Litster, Coating mass distribution from a spouted bed seed coater: experimental and modelling studies, Powder Technol. 74 (1993) 259-270.

[26] A. Kalbag, C. Wassgren, Inter-tablet coating variability: Tablet residence time variability. Chem. Eng. Sci. 64(11) (2009) 2705–2717.

[27] J.P. Kennedy, P.J. Niebergall, Preliminary assessment of an image analysis method for the evaluation of pharmaceutical coatings, Pharm. Dev. Technol. 2(3) (1997) 205-212.

[28] A. Dubey, G. Keyvan, R. Hsai, K. Saranyeas, D. Brone, T. Misra, F.J. Muzzio, Analysis of pharmaceutical tablet coating uniformity by laser-induced breakdown spectroscopy (LIBS), J. Pharm. Innovation 6 (2011) 77–87.

[29] M. Andersson, M. Josefson, F.W. Langkilde, K-G Wahlund, Monitoring of a film coating process for tablets using near infrared reflectance spectrometry, J. Pharm. Biomed. Anal. 20(1-2) (1999) 27-37.

[30] S. Romero-Torres, J.D. Perez-Ramos, K.R. Morris, E.R. Grant, Raman spectroscopic measurement of tablet-to-tablet coating variability, J. Pharm. Biomed. Anal. 38 (2005) 270-274.

[31] J.D. Kirsch, J.K. Drennen, Determination of film-coated tablet parameters by mean-infrared spectroscopy, J. Pharm. Biomed. Anal. 13 (1995) 1273-1281.

[32] L. Mauer, H. Leuenberger, Terahertz pulsed imaging and near infrared imaging to monitor the coating process of pharmaceutical tablets, Int. J. Pharm. 370 (2009) 8-16.

[33] L. Ho, R. Muller, M. Romer, K.C. Gordon, J. Heinamaki, P. Kleinebudde, M. Pepper, T. Rades, Y.C. Shen, C.J. Shachan, P.F. Taday, J.A. Zeitler, Analysis of sustained-release tablet film coats using terahertz pulsed imaging, J. Controlled Release 119 (2007) 253-261.

[34] H. Lin, R.K. May, M.J. Evans, S. Zhong, L.F. Gladden, Y. Shen, J.A. Zeitler, Impact of processing conditions on inter-tablet coating thickness variations measured by terahertz in-line sensing, J. Pharm. Sci. 104 (2015) 2513-2522.

[35] M. Andersson, B. Holmquist, J. Lindquist, O. Nilsson, K.G. Wahlund, Analysis of film coating thickness and surface area of pharmaceutical pellets using fluorescence microscopy and image analysis, J. Pharm. Biomed. Anal. 22 (2000) 325-339.

[36] L. Atares, F. Depypere, J.G. Pieters, K. Dewettinck, Coating quality as affected by core particle segregation in fluidised bed processing, J. Food Eng. 113 (2012) 415-421.

[37] F. Depypere, P. Van Oostveldt, J.G. Pieters, K. Dewettinck, Quantification of microparticle coating quality by confocal laser scanning microscopy (CLSM), Eur. J. Pharm. Biopharm. 73(1) (2009) 179–186.

[38] R. Mani, D. Kadau, H.J. Herrmann, Liquid migration in sheared unsaturated granular media, Granul. Matter 15(4) (2013) 447–454.

[39] B. Mohan, C. Kloss, J. Khinast, S. Radl, Regimes of liquid transport through sheared beds of inertial smooth particles, Powder Technol. 264, (2014), 377–395.

[40] K. Washino, K. Miyazaki, T. Tsuji, T. Tanaka, A new contact liquid dispersion model for discrete particle simulation, Chem. Eng. Res. Des. 110 (2016) 123-130.

[41] J.C. Crocker, D.G. Grier, Methods of Digital Video Microscopy for Colloidal Studies. J. Coll. Int. Sci. 179 (1996) 298-310.

[42] R.C. Gonzalez, R.E. Woods, Digital Image Processing, third ed., Pearson Prentice Hall, 2008.

[43] P. Pandey, M. Katakdaunde, R. Turton, Modeling weight variability in a pan coating process using monte carlo simulations, AAPS PharmaSciTech 7(4) (2006) E1-E10.

[44] B. Freireich, J. Li, A renewal theory approach to understanding interparticle coating variability, Powder Technol. 249 (2013) 330-338.

[45] N.A. Pohlman, J.M. Ottino, R.M. Lueptow, End wall effects in granular tumblers: From quasi-two-dimensional flow to three-dimensional flow, Phys. Rev. E, 74 (2006) 031305.

[46] L.A. Easo, Liquid dispersion in sheared particulate material, PhD thesis, Purdue University, US (2017)

[47] M.E.D. Urso, C.J. Lawrence, M.J. Adams, Pendular, funicular and capillary bridges: Results for two dimensions, J. Coll. Int. Sci. 220 (1999) 42-56.

[48] D. Lievano, S. Velankar, J.J. McCarthy, The rupture force of liquid bridges in two and three particle systems, Powder Technol. 313 (2017) 18-26.

[49] P. Golpalkrishnan, I. Manas-Zloczower, D.L. Feke, Modeling time-dependent forces on liquid bridge interactions between dissimilar particles, Adv. Powder Technol. 19 (2008) 277-292.

[50] M.J. Adams, S.A. Johnson, J.P.K. Seville, C.D. Willett, Mapping the influence of gravity on pendular liquid bridges between rigid spheres, Langmuir 18 (2002) 6180-6184.

[51] D.N. Mazzone, G.I. Tardos, R. Pfeffer, The effect of gravity on the shape and strength of a liquid bridge between two spheres, J. Coll. Int. Sci. 113(2) (19986) 544-556.

[52] K. Murase, T. Mochida, Y. Sagawa, H. Sugama, Estimataion on the strength of a liquid bridge adhered to three spheres, Adv. Powder Technol. 19 (2008) 349-367.

[53] V.P. Mehrhota, K.V.S. Sastry, Pendular bond strength between unequal-sized spherical particles, Powder Technol. 25 (1980) 203-214.

[54] O. Pitois, P. Moucheront, X. Chateau, Liquid bridge between two moving spheres: An experimental study of viscosity effects, J. Coll. Int. Sci. 231 (2000) 26-31.

[55] K. Murase, T. Mochida, H. Sugama, Experimental and numerical studies on liquid bridge formed among three spheres, Granul. Matter 6 (2004) 111-119.

[56] B.J. Ennis, J. Li, G.I. Tardos, R. Pfeffer, The influence of viscosity on the strength of an axially strained pendular liquid bridge, Chem. Eng. Sci. 45(10) (1990) 3071–3088.

[57] E. Bayramli, T.G.M. Van de Ven, An experimental study of liquid bridges between spheres in a gravitational field, J. Coll. Int. Sci. 116(2) (1987) 503-310.

[58] Y. Song, R. Turton, Study of the effect of liquid bridges on the dynamic behavior of two colliding tablets using DEM, Powder Technol. 178 (2007) 99-108.

[59] D.N. Mazzone, G.I. Tardos, R. Pfeffer, The behavior of liquid bridges between two relatively moving particles, Powder Technol. 51(1) (1987) 71–83.

[60] P. Darabi, T. Li, K. Pougatch, M. Salcudean, D. Grecov, Modeling the evolution and rupture of stretching pendular liquid bridges, Chem. Eng. Sci. 65 (2010) 4472-4483.

[61] B.J. Ennis, G. Tardos, R. Pfeffer, A microlevel-based characterization of granulation phenomena, Powder Technol. 65(1-3) (1991) 257-272.

[62] M.J. Adams, V. Perchard, The cohesive forces between particles with interstitial liquid, Inst. Chem. Eng. Symp. 91 (1985) 147–160.

[63] J. Litster, B. Ennis, L. Liu, The Science and Engineering of Granulation Processes, Kluwer Academic Publishers, 2004.

[64] J. Litster, Design and processing of particulate products, Cambridge University Press, 2016.

Appendix

Analysis of images of coated particles

To quantify the distribution of the coating on the particles, a suite of self-written image analysis algorithms written in the LabView programming language was used to analyse the colour of individual particles. The LabView Vision Development Module provides an array of image processing and analysis related 'virtual instruments' (VI) that can be assembled along with self-written code, enabling the rapid development of image processing algorithms.

The 24-bit colour images of coated particles are made up of three 8-bit pixel arrays where a pixel value (0 to 255) denotes the recorded intensity of red $R(x, y)$, green $G(x, y)$ and blue $B(x, y)$ light in that portion of the image (see Fig. A1). To evaluate the distribution of the red-dyed coating on the processed particles it is necessary to separate object and background pixels (image segmentation). This is followed by identifying which object pixels belong to an individual particle (object labelling) from which it is possible to analyse the colour distribution across the particles. Details of the steps involved in analysing the colour images are given in the following sections.

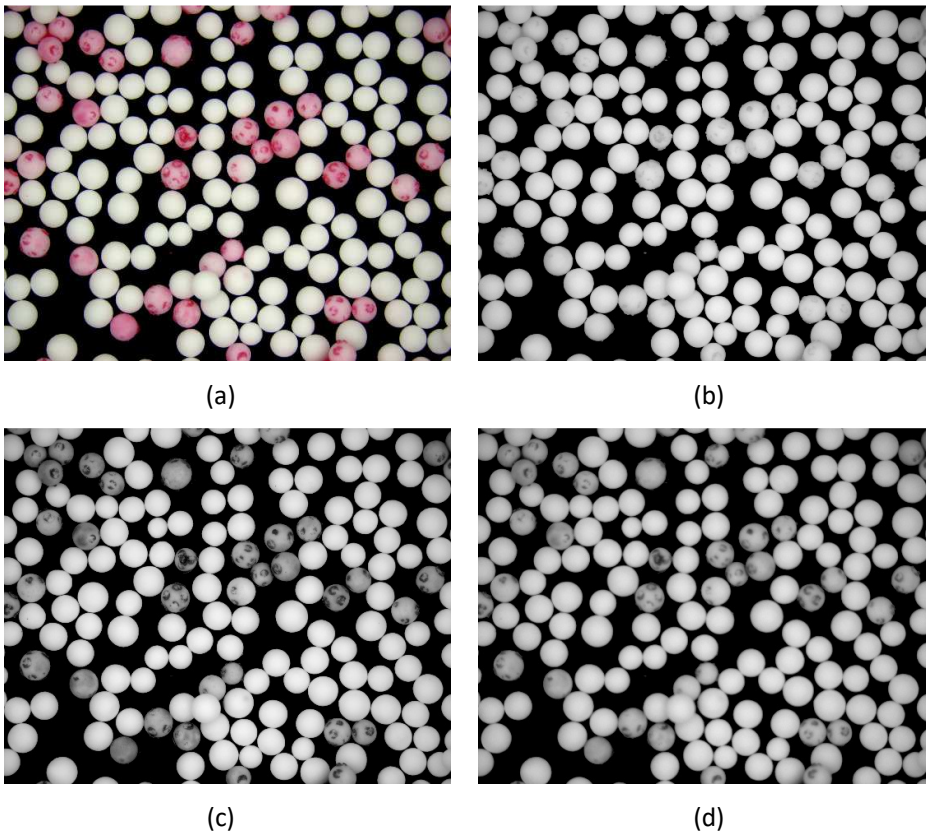

Fig. A1. (a) A typical 24-bit colour image of processed particles where the coating containing the red dye is concentrated on a small number of particles. (b - d) Red, green and blue pixel intensity arrays. The particles that appear red in the colour image are light grey in the red pixel intensity array and dark grey in the blue and green arrays. White particles are nearly equal in intensity across the red, green and blue pixel intensity arrays.

A1. Image pre-processing

Greyscale Image: The operations used to separate object pixels from background pixels require an 8-bit greyscale image. Whilst it is possible to apply the segmentation functions to the red 8-bit pixel intensity array only, a more flexible approach, one that allows for the use of different colour dyes, is to rescale the 24-bit colour image to an 8-bit greyscale image $I(x, y)$. Using the LabView IMAQ Add and IMAQ Multiply VIs the following function is applied:

$$I(x, y) = 0.30\, R(x, y) + 0.59\, G(x, y) + 0.11\, B(x, y). \qquad \text{(A1)}$$

The constants used were chosen to give a close approximation to the brightness of the original colour image (see Fig. A2a). However, it was found that the segmentation functions described below would often remove the darker (red) particles, effectively identifying them as background pixels.

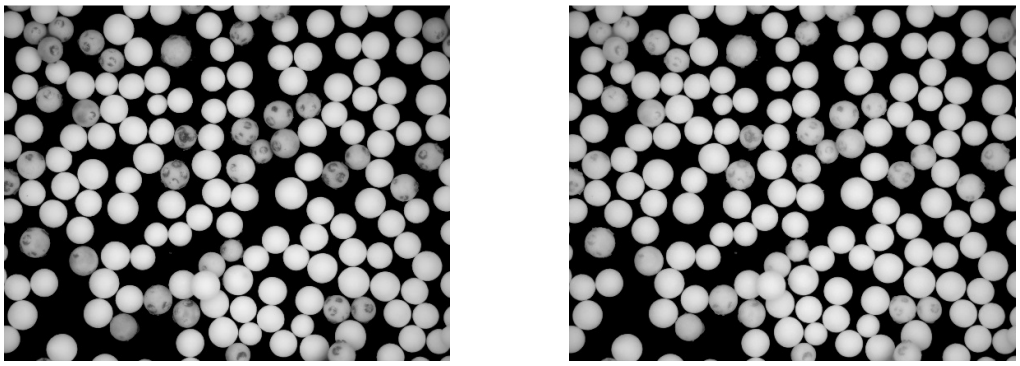

(a) (b)

Fig. A2. Greyscale conversions of image shown in Fig. A1a. (a) Applying typical scaling values to the red, green and blue image intensity arrays results in the red particles being noticeably darker grey than the white particles. (b) Applying a higher than typical scaling value to the red image intensity array results in red particles of similar intensity to the white particles.

Better results were obtained by increasing the brightness of the red particles:

$$I(x,y) = 0.7\,R(x,y) + 0.15\,G(x,y) + 0.15\,B(x,y). \tag{A2}$$

The higher intensity of red pixels results in a greyscale image with red particles of similar brightness to the white particles (see Fig. A2b).

Flat Field Intensity Correction: It was found that the ring light used to illuminate the particles caused a small variation in intensity across the image, from brightest at the centre of the image to darkest at the edges. Auto-thresholding used in image segmentation works best when the illumination is flat. To correct for uneven illumination LabView's IMAQ Flat Field Correction VI was used, supplying it with the greyscale image $I(x,y)$ and a flat field image generated using the IMAQ Estimate Flat Field Model VI. The corrected image $I_{FF}(x,y)$ was used in the next processing step.

Noise Reduction: To suppress noise in the image, the method described by Crocker and Grier [41] was followed and applied a low-pass filter with a Gaussian kernel to the image:

$$I_{\lambda_n}(x,y) = \frac{1}{B}\sum_{i,j=-w}^{w} I_{FF}(x+i, y+j)\, exp\left(-\frac{i^2+j^2}{4\lambda_n^2}\right). \tag{A3}$$

$$R \le w \le 2R \tag{A4}$$

The effect of the filter is to slightly blur the image with the degree of blurring controlled by the noise correlation length λ_n. Typically, $\lambda_n = 2$ was used. The size of the Gaussian kernel is set by the integer w and was set to a value larger than a typical particle radius R in pixels but less than the particle diameter $2R$ ($w \approx 95$). The normalisation parameter is given by $B = \left[\sum_{i=-w}^{w} exp\left(-\left(i^2/4{\lambda_n}^2\right)\right)\right]^2$. Applying the filter requires the output image $I_{\lambda_n}(x, y)$ to be cast as an array of floating point values.

A2. Image segmentation

Boxcar Average: A first pass at separating object pixels from the background pixels was made using a box car average function [41]:

$$I_{BC}(x, y) = \frac{1}{(2w+1)^2} \sum_{i,j=-w}^{w} I(x + i, y + j). \quad \text{(A5)}$$

The function (Eq. (2)) outputs an image $I_{BC}(x, y)$ that models the local average pixel intensities. Subtracting the boxcar image from the smoothed image (Eq. (6)) suppresses the background pixel intensities to 0:

$$I_{\lambda_n - BC}(x, y) = I_{\lambda_n}(x, y) - I_{BC}(x, y), \quad \text{(A6)}$$

After subtracting the boxcar image from the smoothed image, the IMAQ Threshold VI was applied to the image using a threshold of 1. The VI outputs an 8-bit binary image $I_T(x, y)$, where all pixels in $I_{\lambda_n - BC}(x, y)$ with a grey value above 1 are set to 1 and the remainder set to 0 (see Fig. A3a).

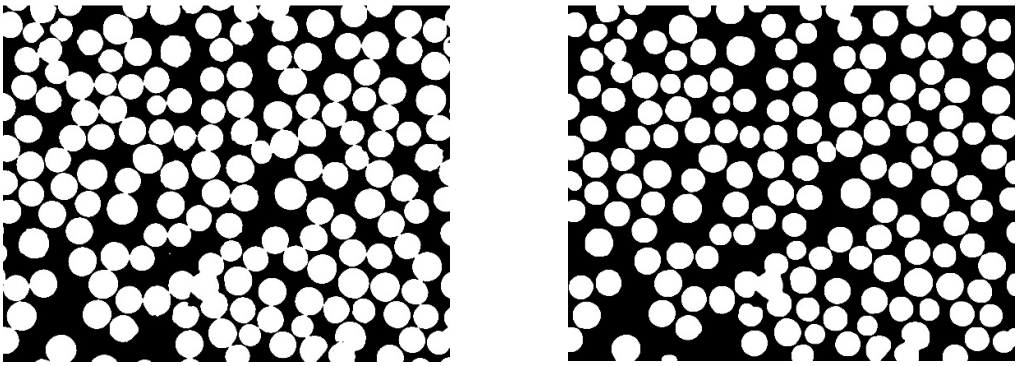

(a) (b)

Fig. A3. (a) Binary image of particles after boxcar subtraction and thresholding. Many touching particles are not fully separated in the binary image. (b) After a series of 'erode' and 'dilate' steps most of the particles in the binary image are now separated. 'Blobs' of connected white pixels correspond to the pixels forming the image of individual particles. Where they are surrounded by black background pixels the segmentation process has been successful. A small number of particles that overlap their neighbours are not fully separated.

Erode and Dilate: Many of the particles in the binary image $I_T(x, y)$ are still connected to their neighbours by a few pixels. Erode and Dilate are two morphological operations that take a 'structuring element' to erode regions of object pixels in a binary image and grow or dilate those regions. By dilating object regions after eroding them it is possible to separate connected regions [42]. Two iterations of the morphological operation 'erode', using the IMAQ Morphology VI with a circular structuring element (width = 43 pixels) were applied. This was followed by 6 iterations of 'dilate' using the IMAQ Morphology VI, using a circular structuring element (width = 13 pixels). The result (see Fig. A3b) was that it was able to separate most of the particles in the binary image $I_{ED}(x, y)$ with minimal loss of pixel data.

A3. Colour analysis

The LabView VI IMAQ Label takes a binary image $I_{ED}(x, y)$ and labels each separate region with a unique grey value (Fig. A4a). This enables the identification of individual particles and their pixels in the image by their label number (see Fig. A4b).

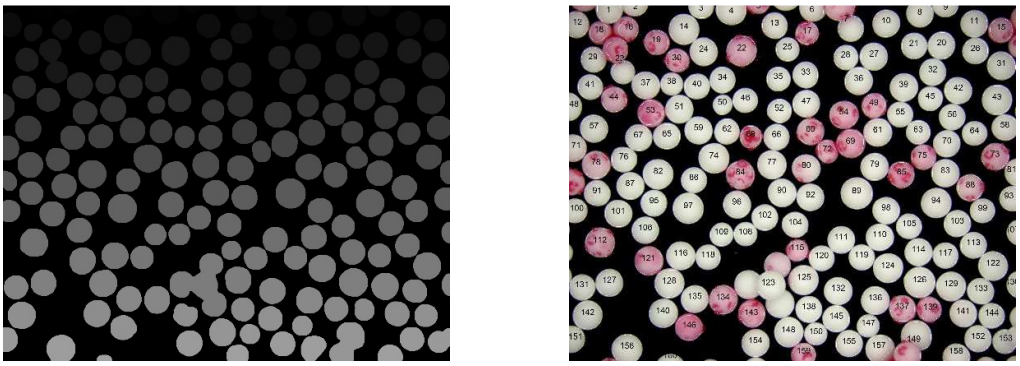

(a) (b)

Fig. A4. (a) A connected region labelled image where each 'blob' in the binary image (Fig. A3) is labelled with a unique grey value. This image is used to identify object pixels in the original image. (b) Original colour image displaying the connected region label number and the outline of the region.

To calculate the red (φ_{R_N}), green (φ_{G_N}) and blue (φ_{B_N}) intensity fractions for an individual particle with label N, the locations of all the pixels labelled N were identified and histograms for the corresponding pixels in the red, green and blue intensity arrays generated ($H_{R_N}(g)$, $H_{G_N}(g)$ and $H_{B_N}(g)$). The intensity fractions were calculated using

$$\varphi_{R_N} = \frac{\sum_{g=1}^{255} H_{R_N}(g)g}{\sum_{g=1}^{255} H_{R_N}(g)g + \sum_{g=1}^{255} H_{G_N}(g)g + \sum_{g=1}^{255} H_{B_N}(g)g}, \quad \text{(A7)}$$

$$\varphi_{G_N} = \frac{\sum_{g=1}^{255} H_{G_N}(g)g}{\sum_{g=1}^{255} H_{R_N}(g)g + \sum_{g=1}^{255} H_{G_N}(g)g + \sum_{g=1}^{255} H_{B_N}(g)g}, \quad \text{(A8)}$$

$$\varphi_{B_N} = \frac{\sum_{g=1}^{255} H_{B_N}(g)g}{\sum_{g=1}^{255} H_{R_N}(g)g + \sum_{g=1}^{255} H_{G_N}(g)g + \sum_{g=1}^{255} H_{B_N}(g)g}. \quad \text{(A9)}$$

For white particles $\varphi_{R_N} \approx \varphi_{G_N} \approx \varphi_{B_N} \approx 0.33$ and for particles that appear in red in the image $\varphi_{G_N} \approx \varphi_{B_N} < \varphi_{R_N}$.